2013 IEEE/RSJ International Conference on
Intelligent Robots and Systems (IROS)
November 3-7, 2013. Tokyo, Japan

An Energy-Efficient High Performance Motion Control of a Hydraulic Crane Applying Virtual Decomposition Control

Janne Koivumäki and Jouni Mattila

***Abstract*— Hydraulic actuators are well-known for their high power-to-weight ratio, rapid responses, compactness and reliable performance. However, one of the drawbacks of fluid power systems have been large energy losses. In this paper, our research objective is to develop both energy-efficient and high performance motion controller for heavy-duty hydraulic manipulators. We apply an unconventional Servo Meter-In Meter-Out (SMIMO) hydraulic valve control set-up that is used to decouple hydraulic actuator load pressure level from load force to improve energy efficiency. The developed control system is based on the Virtual Decomposition Control (VDC) approach to guarantee the closed-loop system stability of the multi degree of freedom heavy-duty hydraulic crane driven by the proposed novel SMIMO VDC controller. Capability for approximately 42% lower energy consumption was achieved in the Cartesian motion trajectory experiments with the proposed novel controller compared with a conventional 4-way servo valve set-up, without significant control performance deterioration.**

I. Introduction

Hydraulic actuators are well-known for their high power-to-weight ratio, rapid responses, compactness and reliable performance. The major advantage of hydraulically driven manipulators is that their payload-to-own-weight ratio can easily be more than one. Therefore, hydraulic manipulators are widely used especially in non-stationary applications, e.g., a hydraulic crane that is installed to an off-highway vehicle or to a working machine. Only very recently, few state-of-the-art small scale and few kg payload electric robots have been developed, e.g., for space applications, reaching a payload-to-own-weight ratio close to one [1]. A hydraulic manipulator we study in this paper has a workspace reach of 3 meters and a payload of 475 kg. The hydraulic manipulator´s own weight is about 260 kg, giving a payload-to-own-weight ratio of 1.8.

Compared to electrical systems, one of the drawbacks of fluid power systems have been large energy losses. Especially in heavy-duty hydraulic applications large energy losses can cause high operating costs, and thus efforts to reduce energy losses are desirable. Nevertheless, as discussed in [2], more energy-efficient hydraulic control systems have usually been characterized by slow response and stability problems. Therefore, high performance but still reasonably energy-efficient motion controls of hydraulic systems remain a formidable problem.

The fundamental difference between electric and hydraulic actuators is that electric actuators are essentially torque sources whereas hydraulic actuators are inherently velocity sources [2], [3]. Hydraulic actuators have also highly nonlinear dynamical behavior which translates to indirect and nonlinear relation between control valve input and actuator force output. Thus, the general control methods that neglect actuator dynamics cannot be applied effectively into hydraulic manipulators [3]. Furthermore, it is considered difficult and time-consuming to determine the uncertain parameters of hydraulic systems´ mathematical models, such as valve characteristics [4]. In addition, the nonlinearities of coupled mechanical linkage dynamics in multi Degree of Freedom (DOF) manipulation pose special challenges for controller design [5].

Due to the challenges described above, in multi DOF hydraulic manipulation it is inevitable to utilize nonlinear model-based control methods in order to achieve high performance motion control. Nevertheless, one of the major challenges in nonlinear model-based control of hydraulic applications has been the lack of stability proofs for the proposed control laws [3]. In fact, only few hydraulic control approaches reported, e.g., [3], [6] and [7] provide guaranteed multi DOF stability.

The Virtual Decomposition Control (VDC) approach has been recently reported, e.g., in [7], [8] and [9], to be an efficient control approach towards high performance control of complex systems, while guaranteeing the system stability. In our previous study [9], the VDC approach was implemented into multi DOF hydraulic crane with the target to achieve a stable and high performance trajectory tracking controller. The results were compared to similar studies reported in [10], [11], and [12] utilizing a simple but effective performance indicator (the ratio of the maximum position tracking error to the maximum velocity), and the developed VDC controller showed outstanding performance improvements in [9].

In this paper, our objective is to design a hydraulic motion controller system that is both energy-efficient and high performance. We utilize an unconventional Servo Meter-In Meter-Out (SMIMO) control set-up that is used to decouple the hydraulic actuator load pressure level from the load force [2], [13]. This allows the individual control of the hydraulic actuator chamber pressures for improving energy efficiency. The developed control system is based on the VDC approach to guarantee closed-loop system stability of the multi DOF heavy-duty hydraulic crane.

*This work was supported by the Academy of Finland under the project "Sensory Network Based Intelligent Condition Monitoring of Mobile Machinery", grant no. 133273.

Janne Koivumäki and Jouni Mattila are at the Dept. of Intelligent Hydraulics and Automation (IHA), Tampere University of Technology (TUT), e-mail: janne.koivumaki@tut.fi.

978-1-4673-6357-0/13/$31.00 ©2013 IEEE

II. VIRTUAL DECOMPOSITION CONTROL

The bases of the implementation of the VDC approach into the studied hydraulic crane have been extensively discussed and shown in our previous study [9]. In this paper the nature of VDC is only described briefly, and thus [9] is highly recommended for reader. The original profound theory of the VDC approach can be found in [7].

The essence of the VDC approach is that the controller uses the dynamics of subsystems rather than the dynamics of the entire system, thus allowing the control problem of the entire system to be converted into the control problem of individual subsystems, while rigorously guaranteeing the stability of entire system. The benefit of the VDC approach comes from the fact that no matter how complicated the original system, the dynamics of subsystems remain relatively simple with fixed dynamics structures invariant to the target system. [7]

In the VDC approach the original system is first virtually decomposed into subsystems, i.e. *objects* and *open chains*, by placing conceptual *virtual cutting points* (VCP) and is then represented by a simple oriented graph which is used to describe the dynamic interactions among subsystems. Moreover, the VCP is interpreted simultaneously as a *driving cutting point* by one subsystem (from which the force/moment vector is exerted) and as a *driven cutting point* (to which the force/moment vector is exerted) for another subsystem. [7]

After defining the required control equations for the decomposed subsystems and for joints to be controlled, the natural concern is on the properties each subsystem should have in order to maintain the stability of the entire system. A feature of the VDC approach is the introduction of a scalar term, namely *Virtual Power Flow* (VPF), at every VCP at which virtual "disconnection" is placed. The VPFs uniquely define the dynamic interactions among the subsystems, playing a vital role in the definition of *virtual stability* of the subsystems. The VPF is defined in [7] as

Definition 1. *The virtual power flow with respect to frame* $\{\mathbf{A}\}$ *can be defined as the inner product of the linear/angular velocity vector error and the force/moment vector error as*

$$p_{\mathbf{A}} = \left({}^{\mathbf{A}}V_r - {}^{\mathbf{A}}V \right)^T \left({}^{\mathbf{A}}F_r - {}^{\mathbf{A}}F \right) \tag{1}$$

where ${}^{\mathbf{A}}V_r \in \mathbb{R}^6$ *and* ${}^{\mathbf{A}}F_r \in \mathbb{R}^6$ *represent the required vectors of* ${}^{\mathbf{A}}V \in \mathbb{R}^6$ *and* ${}^{\mathbf{A}}F \in \mathbb{R}^6$*, respectively.*

Moreover, the following definition from [7] provides a *virtual stability* of a subsystem.

Definition 2. *A subsystem is said to be virtually stable with its affiliated vector* $\boldsymbol{x}(t)$ *being a virtual function in* L_∞ *and its affiliated vector* $\mathbf{y}(t)$ *being a virtual function in* L_2*, if and only if there exists a non-negative accompanying function*

$$\upsilon(t) \geq \frac{1}{2}\boldsymbol{x}(t)^T \mathbf{P} \boldsymbol{x}(t) \tag{2}$$

such that

$$\dot{\upsilon}(t) \leq -\boldsymbol{y}(t)^T \mathbf{Q} \boldsymbol{y}(t) - s(t) + \sum_{\{\mathbf{A}\}\in\Phi} p_{\mathbf{A}} - \sum_{\{\mathbf{C}\}\in\Psi} p_{\mathbf{C}} \tag{3}$$

holds, subject to

$$\int_0^\infty s(t)\,d\tau \geq -\gamma_s \tag{4}$$

with $0 \leq \gamma_s < \infty$*, where* $\mathbf{P}$ *and* $\mathbf{Q}$ *are two block-diagonal positive-definite matrices, set* Φ *contains frames being placed at the driven cutting points of subsystem and set* Ψ *contains frames being placed at the driving cutting points of subsystem, and* $p_{\mathbf{A}}$ *and* $p_{\mathbf{C}}$ *denote the virtual power flows by Definition 1.*

More importantly, if every subsystem of the original system is guaranteed to be virtually stable, this will eventually lead to the L_2 and L_∞ stability of the entire system according to Theorem 2.1 in [7].

III. INDEPENDENT METER-IN METER-OUT CONTROL OF HYDRAULIC CYLINDERS

Traditionally a 4-way directional valve set-up is used to control each hydraulic cylinder of a system. In this conventional control set-up, represented in Fig. 1, a fluid flow is directed through the 4-way (servo) valve to the selected cylinder chamber while another chamber is synchronously connected to return line. The cylinder chambers' fluid in-flow and fluid out-flow are controlled with mechanically connected meter-in and meter-out orifices of the servo valve. In this kind of control arrangement the mechanical connection between valve meter-in and meter-out orifices leads to unnecessary losses in meter-out orifice since fixed valves have to be sized for the worst case scenario which is called over-running load. In this single input control signal arrangement, the load pressure (i.e. the difference between two cylinder chamber pressures scaled by cylinder piston area ratio) is controllable, unlike individual chamber pressures [2].

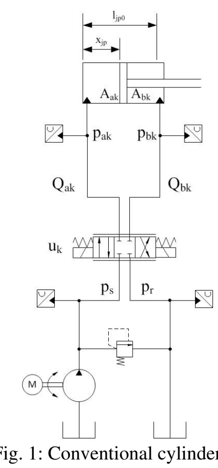

Fig. 1: Conventional cylinder 4-way servo control set-up for the *k*th cylinder.

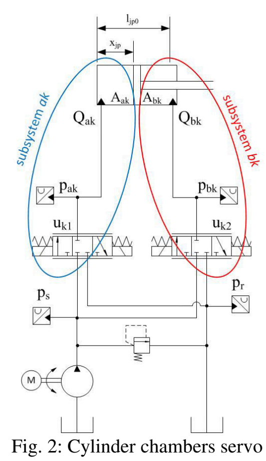

Fig. 2: Cylinder chambers servo meter-in meter-out control set-up for the *k*th cylinder.

Independent metering and individual metering systems are recently discussed, e.g., in [2], [13], and [14], and are referred to as an effective way to arrange an energy-efficient motion control for hydraulic cylinder. In independent metering a mechanical connection between meter-in and meter-out orifices is removed, which enables the individual control of cylinder chamber pressure levels with two independent control valve input signals. When comparing this highly nonlinear two-input two-output system to a conventional cylinder 4-way servo control systems, inter alia a three interesting characteristic features of independent metering systems can be listed: metering losses reduction, dynamic response improvements and stability improvements [13]. Important features of energy recuperation and energy regeneration abilities fall out of the scope of this paper.

As discussed, e.g., in [13], independent metering can be implemented in various ways and with different kinds of valves and layouts, which all have their own pros and cons. The selected independent metering method utilized in this study is illustrated in Fig. 2. In this control set-up both cylinder chambers are controlled with an individual 3-way servo valve. Cylinder chamber pressures individual control leads to the fact that the required cylinder piston output force can be generated with an infinite number of chamber pressure combinations.

IV. Control of the Studied Hydraulic Crane

The hydraulic manipulator system studied in this paper is shown in Fig. 3. The studied system is actuated with two hydraulic cylinders, thus proving 2-DOF motion in the vertical plane. As can be seen in Fig. 3 the studied system is first virtually decomposed into *objects* and *closed chains*, and *closed chains* are further decomposed into *open chains*.

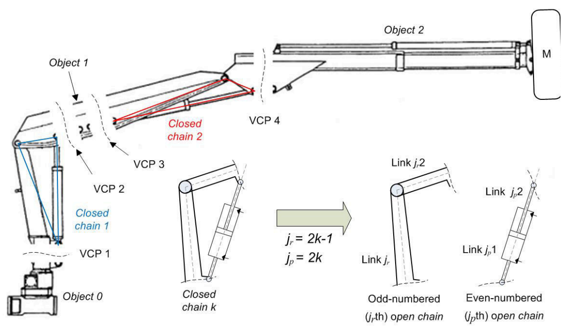

Fig. 3: The studied system with *virtual cutting points*.

A simple oriented graph of the decomposed system is illustrated in Fig. 4.

Referring to our previous study [9], the kinematics, dynamics and control equations for all *objects* and *rigid links* in *open chains* have remained unchanged in this study, and are thus not discussed here. Nevertheless, the control of the kth hydraulic cylinder, $\forall k \in \{1,2\}$, (i.e. actuated even-numbered *open chain*) was arranged in [9] by utilizing the conventional 4-way servo valve set-up (see Fig. 1), whereas the control objective of this paper is on utilizing the independent SMIMO control set-up (see Fig. 2). In order to integrate the discussed cylinder SMIMO control set-up to the VDC approach, the kth hydraulic cylinder needs to be further decomposed into two separate subsystems, namely subsystem *ak* and subsystem *bk* (shown in blue and red in Fig. 2).

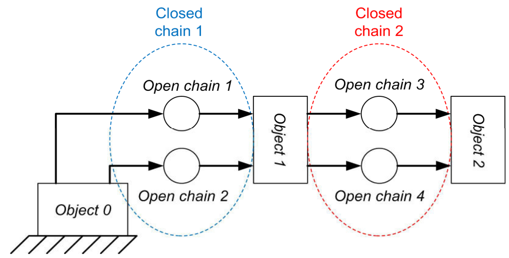

Fig. 4: A simple oriented graph of the studied system.

In the following subsections, a friction model, hydraulic fluid dynamics and control equations for the kth hydraulic cylinder are given. In order to clarify the mathematical notation, the subscript "k" to describe the number of the kth hydraulic cylinder is dropped out from the following equations.

A. Friction model and pressure-induced force

As mentioned in, e.g., [2] and [7], the piston friction makes a large difference between the cylinder output force and chamber pressure-induced force. In order to achieve appropriate piston output force control, it is necessary to implement a suitable friction model. Thus a chamber pressure-induced force f_p of the kth cylinder is defined as

$$f_p = f_c + \mathbf{Y}_f \boldsymbol{\theta}_f \tag{5}$$

where f_c denotes the output force of the kth cylinder and $\mathbf{Y}_f \boldsymbol{\theta}_f$ denotes the linear parametrisized friction model defined in [11].

The chamber pressure-induced force f_p in (5) can be decomposed to chamber pressure force components f_a and f_b as

$$\begin{aligned} f_p &= f_a - f_b \\ &= A_a p_a - A_b p_b \end{aligned} \tag{6}$$

where A_a and A_b denote effective piston areas of chamber *ak* and chamber *bk*, respectively, and p_a and p_b denote the chamber *ak* and chamber *bk* pressures, respectively.

B. Hydraulic fluid dynamics

The flow rates Q_a and Q_b entering into/out from the chambers *ak* and *bk*, respectively, can be written as

$$Q_a = c_{p1} \upsilon(p_s - p_a) u_1 S(u_1) + c_{n1} \upsilon(p_a - p_r) u_1 S(-u_1) \tag{7}$$

$$Q_b = c_{p2} \upsilon(p_s - p_b) u_2 S(u_2) + c_{n2} \upsilon(p_b - p_r) u_2 S(-u_2) \tag{8}$$

where c_{p1} and c_{n1} are two flow coefficients of chamber *ak* control valve, c_{p2} and c_{n2} are two flow coefficients of chamber *bk* control valve, u_1 and u_2 are control voltages of valve *ak* and valve *bk*, respectively. p_s is a system supply pressure, p_r is a pressure of system fluid return line, $S(u)$ is a selective function defined, e.g., in [11], and $\upsilon(\Delta p)$ is a pressure-drop related function defined as

$$\upsilon(\Delta p) = \begin{cases} sign(\Delta p)\sqrt{|\Delta p|} & if\ \Delta p \neq 0\ Pa \\ 0.1\ Pa & if\ \Delta p = 0\ Pa \end{cases} \tag{9}$$

The pressure dynamics of the chamber *ak* and the chamber *bk* can be written as

$$\dot{p}_a = \frac{\beta}{A_a \cdot x_{j_p}}\left(Q_a - A_a \cdot \dot{x}_{j_p}\right) = \frac{\beta}{A_a}\left(u_{fa} - \frac{A_a \cdot \dot{x}_{j_p}}{x_{j_p}}\right) \tag{10}$$

$$\dot{p}_b = \frac{\beta}{A_b\left(l_{j_p0} - x_{j_p}\right)}\left(Q_b + A_b \cdot \dot{x}_{j_p}\right) = \frac{\beta}{A_b}\left(u_{fb} + \frac{A_b \cdot \dot{x}_{j_p}}{\left(l_{j_p0} - x_{j_p}\right)}\right), \tag{11}$$

respectively. In (10) and (11) β denotes the bulk modulus of fluid, x_{j_p} and $\dot{x}_{j_p}$ are a piston position and a piston velocity of the *k*th cylinder, respectively, and l_{j_p0} denotes a maximum stroke of piston of the *k*th cylinder. Furthermore, the control valve voltage related terms u_{fa} and u_{fb} can be written as

$$u_{fa} = \frac{c_{p1}\upsilon\left(p_s - p_a\right)}{x_{j_p}} u_1 S\left(u_1\right) + \frac{c_{n1}\upsilon\left(p_a - p_r\right)}{x_{j_p}} u_k S\left(-u_k\right) \tag{12}$$

$$u_{fb} = \frac{c_{p2}\upsilon\left(p_s - p_b\right)}{l_{j_p0} - x_{j_p}} u_2 S\left(u_2\right) + \frac{c_{n2}\upsilon\left(p_b - p_r\right)}{l_{j_p0} - x_{j_p}} u_2 S\left(-u_2\right) \tag{13}$$

Now, the control valves voltages u_1 and u_2 can be solved from (12) and (13) as

$$u_1 = \frac{x_{j_p}}{c_{p1}\upsilon(p_s - p_a)} u_{fa} S\left(u_{fa}\right) + \frac{x_{j_p}}{c_{n1}\upsilon(p_a - p_r)} u_{fa} S\left(-u_{fa}\right) \tag{14}$$

$$u_2 = \frac{l_{j_p0} - x_{j_p}}{c_{p2}\upsilon(p_s - p_b)} u_{fb} S\left(u_{fb}\right) + \frac{l_{j_p0} - x_{j_p}}{c_{n2}\upsilon(p_b - p_r)} u_{fb} S\left(-u_{fb}\right) \tag{15}$$

Note that (9) together with the assumption that $0 < x_{j_p} < l_{j_p0}$ provides non-singular solutions for (12), (13), (14) and (15), leading to a univalences between (12) and (14), and between (13) and (15).

C. Control Equations

In view of (5), the required chamber pressure-induced force of *k*th cylinder can be written as

$$f_{pr} = f_{cr} + \mathbf{Y}_f \boldsymbol{\theta}_f \tag{16}$$

where f_{cr} denotes the known required output force of the *k*th cylinder (see (33) in [9]). Furthermore, the above required chamber pressure-induced force can be decomposed into the required chamber pressure forces as

$$\begin{aligned} f_{pr} &= f_{ar} + f_{br} \\ &= A_a p_{ar} + A_b p_{br} \end{aligned} \tag{17}$$

where p_{ar} and p_{br} denote the required chamber pressures. The detailed design for p_{ar} and p_{br} will be addressed in section VI.

In view of the chamber pressure dynamics given in (10) and (11), the desired values for control valve related terms u_{fad} and u_{fbd} can be written as

$$u_{fad} = \frac{A_a}{\beta}\dot{p}_{ar} + \frac{A_a \cdot \dot{x}_{j_p}}{x_{j_p}} + k_{fa}(f_{ar} - f_a) + k_x\left(\dot{x}_{j_pr} - \dot{x}_{j_p}\right) \tag{18}$$

$$u_{fbd} = \frac{A_b}{\beta}\dot{p}_{br} - \frac{A_b \cdot \dot{x}_{j_p}}{l_{j_p0} - x_{j_p}} + k_{fb}(f_{br} - f_b) - k_x\left(\dot{x}_{j_pr} - \dot{x}_{j_p}\right) \tag{19}$$

where $k_{fa} > 0$, $k_{fb} > 0$ and $k_x > 0$ denote the cylinder chamber *ak* force error gain, cylinder chamber *bk* force error gain and the piston velocity error gain, respectively. Moreover, $\dot{x}_{j_pr}$ denotes the known required piston velocity of the *k*th cylinder (see (31) in [9]).

Similar to (14) and (15), the control voltages u_1 and u_2 can be written as

$$u_1 = \frac{x_{j_p}}{c_{p1}\upsilon(p_s - p_a)} u_{fad} S\left(u_{fad}\right) + \frac{x_{j_p}}{c_{n1}\upsilon(p_a - p_r)} u_{fad} S\left(-u_{fad}\right) \tag{20}$$

$$u_2 = \frac{l_{j_p0} - x_{j_p}}{c_{p2}\upsilon(p_s - p_b)} u_{fbd} S\left(u_{fbd}\right) + \frac{l_{j_p0} - x_{j_p}}{c_{n2}\upsilon(p_b - p_r)} u_{fbd} S\left(-u_{fbd}\right), \tag{21}$$

respectively.

V. Stability Analysis

As shown in [15], the non-negative accompanying function ν_{j_p} for even-numbered *open chains* ($j_p = 2k, \forall k \in \{1,2\}$), containing two *rigid bodies*, namely link j_p1 (cylinder base) and link j_p2 (piston rod) (see Fig. 3), can be written as

$$\nu_{j_p} = \nu_{j_p1} + \nu_{j_p2} \tag{22}$$

where non-negative accompanying functions of *rigid bodies* can be written as

$$\nu_{j_p1} = \frac{1}{2}\left({}^{\mathbf{B}_{j_p1}}V_r - {}^{\mathbf{B}_{j_p1}}V\right)^T \mathbf{M}_{\mathbf{B}_{j_p1}} \left({}^{\mathbf{B}_{j_p1}}V_r - {}^{\mathbf{B}_{j_p1}}V\right) \tag{23}$$

$$\nu_{j_p2} = \frac{1}{2}\left({}^{\mathbf{B}_{j_p2}}V_r - {}^{\mathbf{B}_{j_p2}}V\right)^T \mathbf{M}_{\mathbf{B}_{j_p2}} \left({}^{\mathbf{B}_{j_p2}}V_r - {}^{\mathbf{B}_{j_p2}}V\right). \tag{24}$$

The time derivative of (22) can be derived to be as

$$\begin{aligned} \dot{\nu}_{j_p} &= \dot{\nu}_{j_p1} + \dot{\nu}_{j_p2} \\ &= -\left({}^{\mathbf{B}_{j_p1}}V_r - {}^{\mathbf{B}_{j_p1}}V\right)^T \mathbf{K}_{\mathbf{B}_{j_p1}} \left({}^{\mathbf{B}_{j_p1}}V_r - {}^{\mathbf{B}_{j_p1}}V\right) \\ &\quad -\left({}^{\mathbf{B}_{j_p2}}V_r - {}^{\mathbf{B}_{j_p2}}V\right)^T \mathbf{K}_{\mathbf{B}_{j_p2}} \left({}^{\mathbf{B}_{j_p2}}V_r - {}^{\mathbf{B}_{j_p2}}V\right) \\ &\quad + p_{\mathbf{B}_{j_p}} - p_{\mathbf{T}_{j_p}} + \left(\dot{x}_{j_pr} - \dot{x}_{j_p}\right)(f_{cr} - f_c) \end{aligned} \tag{25}$$

where $p_{\mathbf{B}_{j_p}}$ and $p_{\mathbf{T}_{j_p}}$ denote the two *virtual power flows* by Definition 1 at the VCPs. In view of Definition 2, the appearance of $\left(\dot{x}_{j_pr} - \dot{x}_{j_p}\right)(f_{cr} - f_c)$ in the right hand side of (25) prevents the virtual stability of the *k*th cylinder, i.e. even-numbered *open chain,* being held at this point.

The following lemma gives a non-negative accompanying function and its time derivative, with respect to fluid dynamics and the respective control equations of the *k*th hydraulic cylinder. The proof for Lemma 1 is given in Appendix A.

Lemma 1. *Consider the kth hydraulic cylinder dynamics described by (5), (6), (10) – (13) and combined with the control equations (16) – (19). The time derivative of*

$$\begin{aligned} \nu_{fdk} &= \nu_{ak} + \nu_{bk} \\ &= \frac{A_a{}^2}{2\beta}(p_{ar} - p_a)^2 + \frac{A_b{}^2}{2\beta}(p_{br} - p_b)^2 \end{aligned} \tag{26}$$

is

$$\begin{aligned} \dot{\nu}_{fdk} &= \dot{\nu}_{ak} + \dot{\nu}_{bk} \\ &\le -k_{fa}\left(f_{ar} - f_a\right)^2 - k_{fb}\left(f_{br} - f_b\right)^2 \\ &\quad -k_x\left(\dot{x}_{j_pr} - \dot{x}_{j_p}\right)\left(f_{cr} - f_c\right) \end{aligned} \tag{27}$$

Now, the following proof ensures the *virtual stability* of the kth hydraulic cylinder comprised of two *rigid bodies* driven by hydraulic fluid.

Proof: The non-negative accompanying function of the kth hydraulic cylinder can be written as

$$\nu_{ck} = \nu_{j_p} + \frac{\nu_{fdk}}{k_x} \tag{28}$$

where ν_{j_p} and ν_{fdk} are defined by (22) and (26), respectively. It follows from (25) and (27) that

$$\begin{aligned}\dot{\nu}_{ck} &= \dot{\nu}_{j_p} + \frac{\dot{\nu}_{fdk}}{k_{xk}} \\ &\le -\left({}^{\mathbf{B}_{jp1}}V_r - {}^{\mathbf{B}_{jp1}}V\right)^T \mathbf{K}_{\mathbf{B}_{jp1}} \left({}^{\mathbf{B}_{jp1}}V_r - {}^{\mathbf{B}_{jp1}}V\right) \\ &\quad -\left({}^{\mathbf{B}_{jp2}}V_r - {}^{\mathbf{B}_{jp2}}V\right)^T \mathbf{K}_{\mathbf{B}_{jp2}} \left({}^{\mathbf{B}_{jp2}}V_r - {}^{\mathbf{B}_{jp2}}V\right) \\ &\quad + p_{\mathbf{B}_{jp}} - p_{\mathbf{T}_{jp}} - \frac{k_{fa}}{k_x}(f_{ar} - f_a)^2 - \frac{k_{fb}}{k_x}(f_{br} - f_b)^2\end{aligned} \tag{29}$$

holds.

Consider the fact that the kth cylinder has one *driving cutting point* associated with frame $\{\mathbf{T}_{j_p}\}$ and one *driven cutting point* associated with frame $\{\mathbf{B}_{j_p}\}$. Now, using (22), (26), (28), (29) and Definition 2 complete the proof of *virtual stability* of the kth hydraulic cylinder.

■

According to Theorem 2.1 in [7], the *virtual stabilities* of all subsystems of the entire decomposed systems will converge to the overall stability of the system. This is because all the VPFs of the entire system will cancel out each other as if each positive VPF (in *driven cutting point*) is connected to its corresponding negative VPF (in *driving cutting point*).

The non-negative accompanying function for the entire hydraulic crane can be written as

$$\nu = \nu_{O_0} + \nu_1 + \nu_{c1} + \nu_{O_1} + \nu_3 + \nu_{c2} + \nu_{O_2} \tag{30}$$

where ν_{O_0}, ν_1, ν_{O_1}, ν_3 and ν_{O_2} denote the non-negative accompanying functions of *object 0*, *open chain 1*, *object 1*, *open chain 3* and *object 2*, respectively, and are further specified in [15]. The time derivative of (30) can now be written in view of [15] and (29), with $j_p = 2k,\ \forall k \in \{1,2\}$, as

$$\begin{aligned}\dot{\nu} \le\ & p_{\mathbf{B}_{CC1}} - p_{\mathbf{B}_1} - p_{\mathbf{B}_2} - \left({}^{\mathbf{B}_1}V_r - {}^{\mathbf{B}_1}V\right)^T \mathbf{K}_{\mathbf{B}_1}\left({}^{\mathbf{B}_1}V_r - {}^{\mathbf{B}_1}V\right) \\ & -\left({}^{\mathbf{B}_{11}}V_r - {}^{\mathbf{B}_{11}}V\right)^T \mathbf{K}_{\mathbf{B}_{11}}\left({}^{\mathbf{B}_{11}}V_r - {}^{\mathbf{B}_{11}}V\right) + p_{\mathbf{B}_1} - p_{\mathbf{T}_1} \\ & -\left({}^{\mathbf{B}_{21}}V_r - {}^{\mathbf{B}_{21}}V\right)^T \mathbf{K}_{\mathbf{B}_{21}}\left({}^{\mathbf{B}_{21}}V_r - {}^{\mathbf{B}_{21}}V\right) \\ & -\left({}^{\mathbf{B}_{22}}V_r - {}^{\mathbf{B}_{22}}V\right)^T \mathbf{K}_{\mathbf{B}_{22}}\left({}^{\mathbf{B}_{22}}V_r - {}^{\mathbf{B}_{22}}V\right) + p_{\mathbf{B}_2} - p_{\mathbf{T}_2} \\ & - \frac{k_{fa1}}{k_{x1}}(f_{a1r} - f_{a1})^2 - \frac{k_{fb1}}{k_{x1}}(f_{b1r} - f_{b1})^2 \\ & -\left({}^{\mathbf{O}_1}V_r - {}^{\mathbf{O}_1}\mathbf{V}\right)^T \mathbf{K}_{\mathbf{O}_1}\left({}^{\mathbf{O}_1}V_r - {}^{\mathbf{O}_1}V\right) + p_{\mathbf{T}_1} + p_{\mathbf{T}_2} - p_{\mathbf{B}_3} - p_{\mathbf{B}_4} \\ & -\left({}^{\mathbf{B}_3}V_r - {}^{\mathbf{B}_3}\boldsymbol{V}\right)^T \mathbf{K}_{\mathbf{B}_3}\left({}^{\mathbf{B}_3}V_r - {}^{\mathbf{B}_3}V\right) \\ & -\left({}^{\mathbf{B}_{31}}V_r - {}^{\mathbf{B}_{31}}V\right)^T \mathbf{K}_{\mathbf{B}_{31}}\left({}^{\mathbf{B}_{31}}V_r - {}^{\mathbf{B}_{31}}V\right) + p_{\mathbf{B}_3} - p_{\mathbf{T}_3} \\ & -\left({}^{\mathbf{B}_{41}}V_r - {}^{\mathbf{B}_{41}}V\right)^T \mathbf{K}_{\mathbf{B}_{41}}\left({}^{\mathbf{B}_{41}}V_r - {}^{\mathbf{B}_{41}}V\right) \\ & -\left({}^{\mathbf{B}_{42}}V_r - {}^{\mathbf{B}_{42}}V\right)^T \mathbf{K}_{\mathbf{B}_{22}}\left({}^{\mathbf{B}_{42}}V_r - {}^{\mathbf{B}_{42}}V\right) + p_{\mathbf{B}_4} - p_{\mathbf{T}_4} \\ & - \frac{k_{fa2}}{k_{x2}}(f_{a2r} - f_{a2})^2 - \frac{k_{fb2}}{k_{x2}}(f_{b2r} - f_{b2})^2 \\ & -\left({}^{\mathbf{O}_2}V_r - {}^{\mathbf{O}_2}\mathbf{V}\right)^T \mathbf{K}_{\mathbf{O}_2}\left({}^{\mathbf{O}_2}V_r - {}^{\mathbf{O}_2}V\right) + p_{\mathbf{T}_3} + p_{\mathbf{T}_4} - p_{\mathbf{G}}\end{aligned} \tag{31}$$

For the given $p_{\boldsymbol{B}_{CC1}} = 0$ (with zero velocity) and $p_{\boldsymbol{G}} = 0$ (with zero force), it can be seen that all the VPFs are cancelled out from (31), leading to the stability of the entire system in the view of Theorem 2.1 in [7].

VI. Experimental Set-Up and Implementation Issues

The experimental set-up consisted of the same set-up described in [9] with the following changes

- Bosch 4WRPEH10 servo valves (100 dm^3/min @ Δp3.5MPa per notch) for cylinder 1
- Parker D3Fplus servo valves (100 dm^3/min @ Δp3.5MPa per notch) for cylinder 2
- Heidenhein ROD 486 incremental encoder with IVB 102 interpolation units for both crane revolute joints providing a piston position resolution < $1.2 \cdot 10^{-3}$ mm.

In the measurements the cylinder chamber control valves were located as close to cylinders as possible in order to minimize the need for hydraulic hosing, thus reducing the overall system flexibilities.

The tuned controller parameters used in this study are given in Table I.

Table I

Controller Parameters

CYLINDER 1	CYLINDER 2
$k_{x1} = 0.04$	$k_{x2} = 0.02$
$k_{fa1} = 5.0 \cdot 10^{-8}$	$k_{fa2} = 4.5 \cdot 10^{-8}$
$k_{fb1} = 5.0 \cdot 10^{-8}$	$k_{fb2} = 7.0 \cdot 10^{-8}$
$\lambda_2 = 11$	$\lambda_4 = 15$
$\mathbf{K_A} = 500 \cdot \mathbf{I_6}$ for all *rigid links* and *objects*	
$c_{p11} = 6.5 \cdot 10^{-8}$ $c_{n11} = 7.5 \cdot 10^{-8}$	$c_{p21} = 7.0 \cdot 10^{-8}$ $c_{n21} = 9.0 \cdot 10^{-8}$
$c_{p12} = 6.5 \cdot 10^{-8}$ $c_{n12} = 7.5 \cdot 10^{-8}$	$c_{p22} = 4.7 \cdot 10^{-8}$ $c_{n22} = 4.5 \cdot 10^{-8}$

As discussed in [2], the steady-state cylinder chamber pressures are complex nonlinear functions of supply pressure, load force, motion direction and valve opening, even if valve leakage flow is neglected. In the experiments the manipulator end-effector was first driven into the desired Cartesian motion trajectory starting point. When the desired starting point was reached, the controlled cylinder chamber pressures were driven into the desired initial pressure levels p_{ad0} and p_{bd0}, satisfying the required chamber pressure-induced force f_{pr0} (see (16) and (17)) in desired Cartesian starting point.

Now, as long as (17) is satisfied, the use of independent SMIMO control set-up enables us to design the required chamber pressures p_{ar} and p_{br} in an infinite number of different combinations. In order to achieve energy-efficient cylinder motion, it is favorable to set the meter-out chamber pressure level as low as reasonably possible while avoiding cavitation problems. The proposed control law for the required chamber pressures to be applied in this study was written as

$$\begin{cases} p_{ar} = p_{ad0} + \alpha_k\left(f_{pr} - f_{pr0}\right) \\ p_{br} = \frac{f_{pr} - A_a \cdot p_{ar}}{-A_b} \end{cases} \tag{32}$$

where α_k denotes the coefficient that transforms the changes in the required chamber pressure-induced force into the required change of chamber *ak* pressure. Note that the required chamber pressure p_{br} is bounded to the required chamber pressure p_{ar}. In the measurements following value for $\alpha_k = \frac{10^5}{460}\frac{Pa}{N}$ was used.

VII. Experimental Results

The aim of the experiments was to compare the proposed novel SMIMO VDC controller developed in Chapter IV to the results obtained with a conventional 4-way servo VDC control set-up reported in [9]. The proposed SMIMO VDC set-up aims at reductions in motion control system energy consumption while maintaining high motion tracking performance. In the experiments, the same rectangular four point Cartesian motion trajectory presented in [9] was driven with three different Cartesian point-to-point transition times, denoted as $t_{f2.5}$, t_{f5} and t_{f10}.

Figs. 5 – 7 illustrate the SMIMO VDC controlled results with hydraulic crane under three different Cartesian point-to-point transition times. In these figures cylinder 1 data is illustrated in red, cylinder 2 data in blue and the required reference trajectories in black color. Note that valve control voltages (third plots) in Fig. 6 and Fig. 7 are given in a different scale compared to Fig. 5 in order to a achieve better view of control valves' behavior.

By comparing the measured data given in Figs. 5 – 7 to the corresponding measurement data in Figs. 10 – 12 from [9], it can be concluded that very similar results are achieved with a cylinder SMIMO VDC control compared to a conventional 4-way servo VDC control. Thus, only the piston position tracking error data (first plots in Figs 5 – 7) is analyzed in this paper.

The maximum piston position tracking errors for cylinder 1 were reported in [9] to be around 0.5 mm for all Cartesian transition times. As shown in Figs 5 – 7, very similar results were achieved for cylinder 1 in this study. By comparing the achieved results of cylinder 2 to results of cylinder 1, it can be seen that the piston position tracking error for cylinder 2 is at maximum 4 times higher than 0.5 mm. In addition, the applied Cartesian transition time seems to have a notable effect on the cylinder 2 position tracking error. The weaker performance of cylinder 2 is most likely caused by defective/inappropriate dynamical behavior of old control valves applied for cylinder 2. The cylinder 2 control valves' flow coefficients (c_{p21}, c_{n21}, c_{p22} and c_{n22}), given in Table I, supports this observation (values should have approx. the same magnitudes with respect to cylinder 1 values).

In studies of Zhu, e.g., [8] and [11], the ratio of the maximum position tracking error $|\Delta x_{max}|$ to the maximum velocity $|v_{max}|$ has been used as a performance indicator for the controller. The results between a conventional 4-way servo VDC control and SMIMO VDC control are given in Table II.

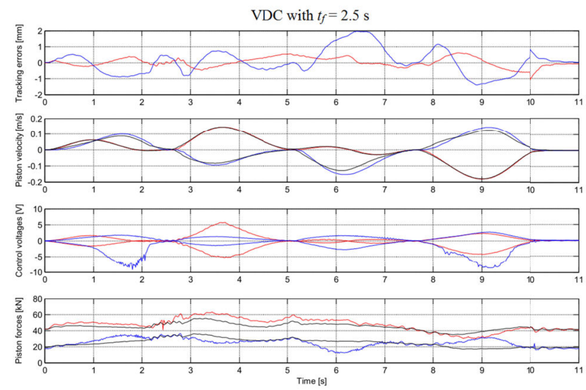

Fig. 5: Measured results under point-to-point Cartesian transition time $t_{f2.5}$.

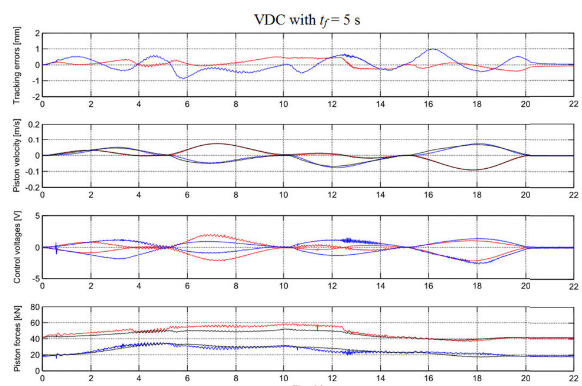

Fig. 6: Measured results under point-to-point Cartesian transition time t_{f5}.

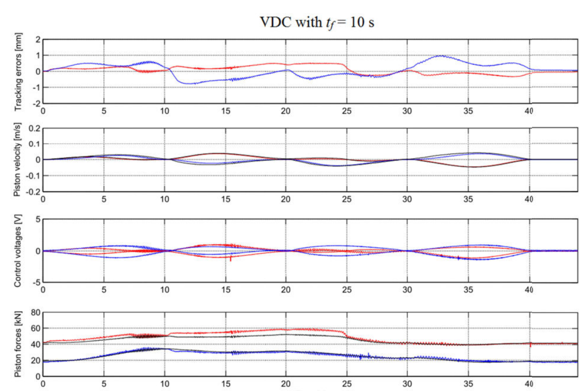

Fig. 7: Measured results under point-to-point Cartesian transition time t_{f10}.

The data given in Table II shows that very similar results with SMIMO VDC control compared to a conventional 4-way servo VDC control were achieved with cylinder 1. The achieved results with cylinder 2 were far more defective with SMIMO VDC control compared to conventional 4-way servo VDC control. In spite of that, the data given by cylinder 1 verifies that with an appropriate tuning it is able to achieve as advantageous control performance with the proposed novel SMIMO VDC controller as with a conventional 4-way servo VDC controller.

TABLE II

COMPARISON OF CONTROLLER PERFORMANCES $\left(\left|\frac{\Delta x_{max}}{v_{max}}\right|\right)$

	Conventional 4-way servo VDC control	Servo meter-in meter-out VDC control
t_f = 2.5s. (Fig. 5)	*Cylinder 1: 0.0037 (s)* *Cylinder 2: 0.0049 (s)*	*Cylinder 1: 0.0060 (s)* *Cylinder 2: 0.0131 (s)*
t_f = 5s. (Fig. 6)	*Cylinder 1: 0.0047 (s)* *Cylinder 2: 0.0062 (s)*	*Cylinder 1: 0.0055 (s)* *Cylinder 2: 0.0129 (s)*
t_f = 10s. (Fig. 7)	*Cylinder 1: 0.0098 (s)* *Cylinder 2: 0.0088 (s)*	*Cylinder 1: 0.0114 (s)* *Cylinder 2: 0.0251 (s)*

The aim of the proposed controller was to achieve an energy-efficient motion control for hydraulic cylinders. Figs. 8 – 10 illustrate the measured chamber pressures (chamber *ak* pressure with red and chamber *bk* pressure with blue) with a conventional 4-way servo VDC control (left-hand side) and with SMIMO VDC control (right-hand side) with three different Cartesian point-to-point transition times. The conventional 4-way servo controlled chamber pressures are from measurements reported in [9] but the uncontrollable individual cylinder chamber pressures were not represented in [9].

The right column plots in Figs. 8 – 10 present SMIMO VDC control results together with the required chamber pressure trajectories generated by (32) in black color. As can be seen in Figs. 8 – 10, the measured chamber pressures track their required reference pressures quite well. Nevertheless, the pressure tracking ability seems to decline when the Cartesian transition time is reduced. In the SMIMO VDC control scheme it was important to ensure that cavitation in cylinder chambers is avoided.

The hydraulic energy used by hydraulic cylinder in the driven cases can be written as

$$E = \int_0^{4t_f} p_{in}(\tau) Q_{in}(\tau) d\tau \tag{33}$$

where $p_{in}(\tau)$ denotes the pressure of meter-in chamber and $Q_{in}(\tau)$ denotes the fluid flow taken from supply line into the meter-in chamber. The calculated energy usages for cylinders in these discussed cases are given in Table III.

As can be seen in Table III, during driven Cartesian motion trajectory, in cylinder 1 approximately 30% less hydraulic energy is taken from the system supply line with SMIMO VDC controlled set-up when compared to a conventional 4-way servo VDC control set-up. With cylinder 2 approximately 55% less hydraulic energy is taken from the system supply line with SMIMO VDC controlled set-up. The total hydraulic energy usage by two hydraulic cylinders during Cartesian motion trajectories was approximately 42% less with SMIMO VDC controlled set-up.

The numbers in Table III are only calculated estimates of the energy saving potential of the proposed SMIMO VDC control scheme. If a constant displacement pump is used, the total system energy efficiencies in these two discussed cases are the

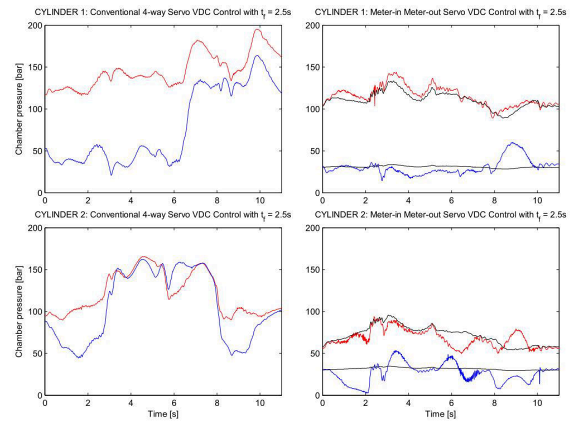

Fig. 8: Chamber pressures of cylinders with a conventional 4-way servo VDC control (left column) and with the proposed SMIMO VDC control (right column) under the Cartesian transition time t_f = 2.5s.

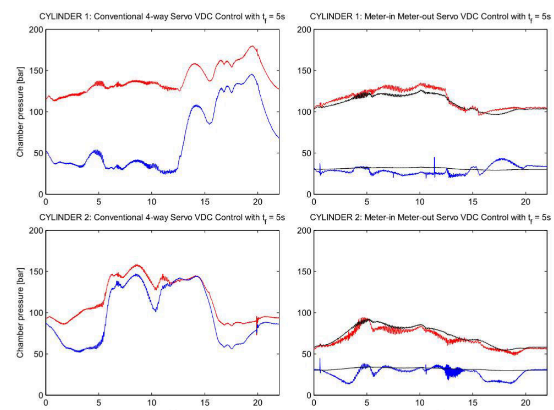

Fig. 9: Chamber pressures of cylinders with a conventional 4-way servo VDC control (left column) and with the proposed SMIMO VDC control (right column) under the Cartesian transition t_f = 5s.

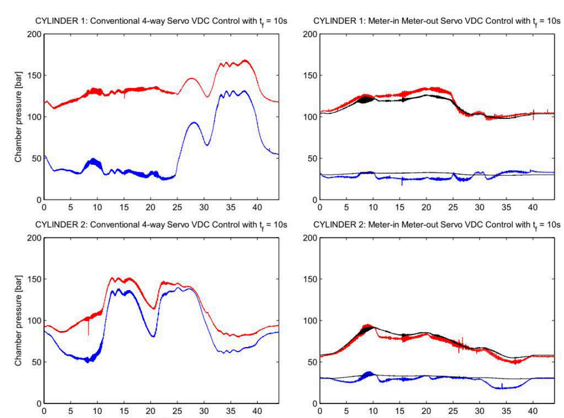

Fig. 10: Chamber pressures of cylinders with a conventional 4-way servo VDC control (left column) and with the proposed SMIMO VDC control (right column) under the Cartesian transition time t_f =10s.

same because energy savings with the SMIMO VDC control are wasted through a pressure relief valve. Nevertheless, as can be seen in Figs. 8 – 10, the pump supply pressure can be set notably lower in SMIMO VDC controlled set-up, which will lead to better energy-efficiency compared to a conventional 4-way servo VDC controlled set-up. In theory, it is possible to achieve almost the same energy efficiency numbers given in Table III by applying a Load-Sensing (LS) pump and the proposed SMIMO VDC control set-up. Nevertheless, as discussed, e.g., in [13], using the LS system with closed loop control the system dynamics become highly under damped, which may cause oscillation and stability problems to the overall system.

TABLE III

COMPARISON OF ENERGY USAGE

	Conventional 4-way servo VDC control	SMIMO VDC control
t_f = 2.5s. (Fig. 8)	*Cyl 1: 30.0 kJ* *Cyl 2: 30.2 kJ*	*Cyl 1: 21.4 kJ* *Cyl 2: 13.9 kJ*
t_f = 5s. (Fig. 9)	*Cyl 1: 28.8 kJ* *Cyl 2: 27.6 kJ*	*Cyl 1: 20.0 kJ* *Cyl 2: 12.3 kJ*
t_f = 10s. (Fig. 10)	*Cyl 1: 28.0 kJ* *Cyl 2: 26.7 kJ*	*Cyl 1: 19.4 kJ* *Cyl 2:12.2 kJ*

VIII. CONCLUSION

In this paper we proposed a novel independent Servo Meter-In Meter-Out (SMIMO) VDC controller for a hydraulic multi DOF manipulator in order to achieve the dual objective of energy saving and high precision motion control. The stability of the developed controller was guaranteed by the stability theory of the VDC approach. By comparing the proposed novel SMIMO VDC controller with a conventional 4-way servo VDC controller, it was demonstrated that approximately 42% smaller energy consumption of hydraulic cylinders is achievable in the Cartesian space motion control experiments presented. Furthermore, it was shown that by an appropriate controller tuning, the proposed controller is able to achieve the same state-of-the-art control performance as was achieved with a conventional 4-way servo VDC controller in [9].

The methods to improve the total energy-efficiency of the high performance hydraulic manipulator systems will be in the scope of the author's future studies.

APPENDIX A

PROOF FOR LEMMA 1

The time derivatives of ν_{ak} and ν_{bk} in (26) can derived to be as

$$\dot{v}_{ak} = (p_{ar} - p_a)\frac{{A_a}^2}{\beta}(\dot{p}_{ar} - \dot{p}_a)$$
$$= (f_{ar} - f_a)\frac{A_a}{\beta}(\dot{p}_{ar} - \dot{p}_a) \tag{34}$$

$$\dot{v}_{bk} = (p_{br} - p_b)\frac{{A_b}^2}{\beta}(\dot{p}_{br} - \dot{p}_b)$$
$$= (f_{br} - f_b)\frac{A_b}{\beta}(\dot{p}_{br} - \dot{p}_b), \tag{35}$$

leading to fact that time derivative of (26) can derived to be in the view of (5), (6), (10) – (13) and (16) – (19) as

$$\begin{aligned}
\dot{v}_{fdk} &= \dot{v}_{ak} + \dot{v}_{bk} \\
&= (f_{ar} - f_a)\frac{A_a}{\beta}(\dot{p}_{ar} - \dot{p}_a) + (f_{br} - f_b)\frac{A_b}{\beta}(\dot{p}_{br} - \dot{p}_b) \\
&= (f_{ar} - f_a)(u_{fad} - u_{fa}) - k_{fa}(f_{ar} - f_a)^2 \\
&\quad - k_x(f_{ar} - f_a)\left(\dot{x}_{j_pr} - \dot{x}_{j_p}\right) + (f_{br} - f_b)(u_{fbd} - u_{fb}) \\
&\quad - k_{fb}(f_{br} - f_b)^2 + k_x(f_{br} - f_b)\left(\dot{x}_{j_pr} - \dot{x}_{j_p}\right) \\
&= (f_{ar} - f_a)(u_{fad} - u_{fa}) - k_{fa}(f_{ar} - f_a)^2 \\
&\quad + (f_{br} - f_b)(u_{fbd} - u_{fb}) - k_{fb}(f_{br} - f_b)^2 \\
&\quad - (f_{pr} - f_p)k_x\left(\dot{x}_{j_pr} - \dot{x}_{j_p}\right) \\
&\leq -k_{fa}(f_{ar} - f_a)^2 - k_{fb}(f_{br} - f_b)^2 \\
&\quad - k_x\left(\dot{x}_{j_pr} - \dot{x}_{j_p}\right)(f_{cr} - f_c)
\end{aligned} \tag{36}$$

REFERENCES

[1] G. Hirzinger, et al. "DLR's torque-controlled light weight robot III – are we reaching the technological limits now?" in *Proc. of the IEEE Int. Conf. on Robotics and Automation (ICRA)*, May 2002, pp. 1710 – 1716.

[2] J. Mattila, *On Energy-Efficient Motion Control of Hydraulic Manipulators,* Ph.D. thesis, Tampere University of Technology, Dec. 2000.

[3] M. R. Sirouspour, S.E. Salcudean, "Nonlinear Control of a Hydraulic Robots", in *IEEE Trans. on Robotic and Automation*, vol. 17, no. 2, Apr. 2001, pp. 759 – 765.

[4] N. Niksefat, N. Sepehri, "Robust Force Controller Design for a Hydraulic Actuator Based on Experimental Input-Output Data*",* in *Proc. of the American Control Conference*, vol. 5, June 1999, pp. 3718 – 3722.

[5] L.Sciavicco, B. Siciliano, *Modeling and Control of a Robot Manipulators*, Springer, London, 2000.

[6] F. Bu, B. Yao, "Observer Based Coordinated Adaptive Robust Control of Robot Manipulators Driven by Single-Rod Hydraulic Actuators", in *Proc. of the IEEE Int. Conf. Robotics and Automation (ICRA)*, Apr. 2000, pp. 3034 – 3039.

[7] W.-H. Zhu, *Virtual Decomposition Control*, Springer-Verlag, 2010.

[8] W.-H. Zhu, G. Vukovich, "Virtual decomposition control for modular robot manipulators", in *IFAC World Congress*, Sept. 2011, vol. 18, pp. 13486 – 13491.

[9] J. Koivumäki, J. Mattila, "Automation of Multi Degree of Freedom Hydraulic Crane by Using a Virtual Decomposition Control" in *Proc.of the IEEE/ASME Int. Conf. on Adv. Intelligent Mechatronics (AIM)*, July 2013, pp. 912 – 919.

[10] J. Mattila, T. Virvalo, "Energy-efficient motion control of a hydraulic manipulators" in Proc. of the *IEEE Int. Conf. on Robotics and Automation (ICRA)*, Apr. 2000, pp. 3000 – 3006.

[11] W.-H. Zhu, J.C. Piedboeuf, "Adaptive output force tracking control of hydraulic cylinders with applications to robot manipulators" *Transactions of the ASME*, vol. 127, June 2005, pp. 206–217.

[12] B.Yao, F.Bu, "Desired compensation adaptive robust control of single-rod electro-hydraulic actuator" in *Proc. of American Control Conference*, June 2001, vol. 5, pp. 3926 – 3931.

[13] B. Eriksson, J-O, Palmberg, "Individual metering fluid power systems: challenges and opportunities", *Proc. of the IMechE, Part I*, vol. 225, no. 2, July 2010, pp. 196 – 211.

[14] S. Liu, B. Yao, "Coordinate control of energy saving programmable valves" *IEEE Trans. on Control System Technology*, Vol. 16, No. 1, Jan. 2008, pp. 34 – 45.

[15] J. Koivumäki, *Virtual decomposition control of a hydraulic manipulator*, M.Sc. Thesis, Tampere University of Technology, Dec. 2012.